J Sol-Gel Sci Technol
DOI 10.1007/s10971-011-2630-5

ORIGINAL PAPER

Fabrication of a high thermal-stable methacrylate-silicate hybrid nanocomposite: hydrolytic versus non-hydrolytic sol–gel synthesis of methacryl-oligosiloxanes

Jungho Jin · SeungCheol Yang · Byeong-Soo Bae

Received: 28 July 2011 / Accepted: 15 November 2011
© Springer Science+Business Media, LLC 2011

Abstract A high thermal-stable methacrylate-silicate hybrid nanocomposite (hybrimer) was fabricated based on UV-induced polymerization of a highly-condensed methacryl-oligosiloxane resin (*Hy*-MO). The *Hy*-MO resin was newly synthesized via an acid-catalyzed hydrolytic sol–gel reaction of 3-(methacryloxy) propyl trimethoxysilane (MPTS) and diphenyldimethoxysilane. The basic properties of *Hy*-MO were compared with a conventional resin prepared by a $Ba(OH)_2{\cdot}H_2O$-catalyzed non-hydrolytic sol–gel reaction of MPTS and diphenylsilanediol (*N*-MO). It was found that *Hy*-MO have a higher siloxane condensation degree, larger molecular size and weight than the *N*-MO due to the highly mobile proton ions that effectively catalyze the overall sol–gel reaction. The resultant *Hy*-MO hybrimer showed a higher thermal stability than *N*-MO hybrimer.

Keywords Sol–gel hybrid nanocomposite · Hydrolytic sol–gel reaction · Siloxane condensation · $Ba(OH)_2{\cdot}H_2O$

1 Introduction

Over the past decade, silicate-based organic/inorganic hybrid materials (OIHMs) have grown into a mature class of materials [1–6]. Because they provide versatile properties not found with their non-hybrid counterparts, silicate-based OIHMs have been utilized in a broad spectrum of applications, such as waveguides [7–10], microlenses [11, 12], functional coatings [13, 14], dielectrics [15–17], lithographies [18–20], and nanocomposites [16, 21–23]. The desirable features of OIHMs, which include high temperature stability, chemical resistance, optical transparency, and ease of functionalization, originate from the synergistically combined natures of the inorganic silicates (or siloxanes) and the organic phase [18, 23]. Such molecular-scale chemical hybridization of the two phases can be effectively achieved by a versatile chemical synthesis method called, the sol–gel process; the mild reaction conditions of the sol–gel process allow for low-temperature processibility and solution processibility [16, 24–26]. To date, via the sol–gel approach, diverse types of OIHMs have been tailored by many research groups on the basis of different terms, such as "ceramers" [24, 25, 27], "ormosils or ormocers" [28], and "hybrimers" [29].

Hybrimers, in particular, are currently under intense studies in relation to manifold practical applications, such as micro-optical devices [12, 30], encapsulant for organic light emitting diodes [31, 32], transparent low-k passivation of thin film transistors [17, 33], electrolytes for dye-sensitized solar cells [34], gas barrier coating for OLEDs [35], and even flexible electronics [36]. Hybrimers can be fabricated by photo-induced or heat-induced polymerization of organo-oligosiloxane resin (Scheme 1). The salient chemistry in the formation of the organo-oligosiloxane resin involves a non-hydrolytic sol–gel reaction of organo-alkoxysilane and diphenylsilanediol (DPSD). Unlike the conventional hydrolytic sol–gel process, where water is necessarily added for hydrolysis prior to condensation, the non-hydrolytic sol–gel process does not require the addition of water, and yet the condensation of siloxane

Electronic supplementary material The online version of this article (doi:10.1007/s10971-011-2630-5) contains supplementary material, which is available to authorized users.

J. Jin · S. Yang · B.-S. Bae (✉)
Laboratory Optical Materials and Coating, Department of Materials Science and Engineering, KAIST, 373-1 Guseong-dong Yuseong-gu, Daejeon, Republic of Korea
e-mail: bsbae@kaist.ac.kr

Published online: 24 November 2011

networks can be completed due to the hydroxyl groups (silanols) of the DPSD. In related studies, Eo et al. [37] and Kim et al. [38] elaborated the non-hydrolytic condensation reaction between a DPSD and a typical organo-alkoxysilane 3-(methacryloxy) propyl trimethoxysilane (MPTS).

The direct condensation between organo-alkoxysilane and DPSD can be effectively catalyzed with barium hydroxide monohydrate ($Ba(OH)_2{\cdot}H_2O$) [37, 38]. A typical crystalline-solid catalyst, $Ba(OH)_2{\cdot}H_2O$ is used in a diverse range of organic reactions, such as Michael addition, Claisen-Schmidt condensation, and transesterification (or methanolysis) in biodiesel synthesis [39–41]. Because of the strong ionization tendency of barium, $Ba(OH)_2{\cdot}H_2O$ serves as a strong base catalyst; basicity level is even stronger than that of potassium hydroxide. Although alkaline-earth metal hydroxides are generally used as a catalyst in conventional sol–gel reactions [26], the exact catalysis mechanism of $Ba(OH)_2{\cdot}H_2O$ in a non-hydrolytic sol–gel reaction is not fully understood. One plausible mechanism of the catalysis of $Ba(OH)_2{\cdot}H_2O$ in a non-hydrolytic condensation between DPSD and organo-alkoxysilane is based on general models pertaining to the base-catalysis of a sol–gel process coupled with the general catalytic role of $Ba(OH)_2{\cdot}H_2O$ in organic reactions. That is, the deprotonation of the silanols of DPSD at the basic surface hydroxyls of $Ba(OH)_2{\cdot}H_2O$ crystal is followed by the formation of siloxane linkages through nucleophilic substitution entailing a release of methanol as a by-product. In this case, the catalysis occurs predominantly at the solid–liquid interfaces (namely the $Ba(OH)_2{\cdot}H_2O$ surface-reactant solution interfaces). We therefore hypothesize that the spatial hindrance in the catalysis, which is caused by the solid $Ba(OH)_2{\cdot}H_2O$, leads to incomplete condensation of the siloxane networks and that the incomplete condensation induces the non-optimal properties of the hybrimer.

In light of the above background, we introduce a novel synthesis of a highly-condensed methacryl-oligosiloxane (MO) resin via an acid-catalyzed hydrolytic sol–gel reaction of MPTS and diphenyldimethoxysilane (DPDMS) for the fabrication of a high-performance hybrimer. We used hydrochloric acid (HCl) as the catalyst and a reflux condenser to promote an effective hydrolysis and condensation reaction between MPTS and DPDMS. In our new system, highly mobile proton ions actively catalyze the overall sol–gel reaction; this process produces more highly-condensed MO than a conventional non-hydrolytic system which uses the $Ba(OH)_2{\cdot}H_2O$. To characterize the degree of siloxane condensation, as well as size and molecular weight of the new MO, we used Fourier transform infrared (FT-IR) analysis, ^{29}Si nuclear magnetic resonance (^{29}Si NMR) analysis, small angle neutron scattering (SANS) and matrix-assisted laser desorption and ionization time-of-flight (MALD-TOF) analysis. The final assessment of the basic thermophysical properties of the resultant hybrimer was made with a dynamic mechanical analyzer (DMA), a thermogravimetric analyzer (TGA), and a dilatometer.

2 Experimental section

2.1 Materials

3-(Methacryloxy) propyl trimethoxysilane (MPTS), barium hydroxide monohydrate ($Ba(OH)_2$-H_2O) and 2,2-dimethoxy-2-phenylacetophenone were purchased from Aldrich (Milwaukee, WI) and used without further purification.

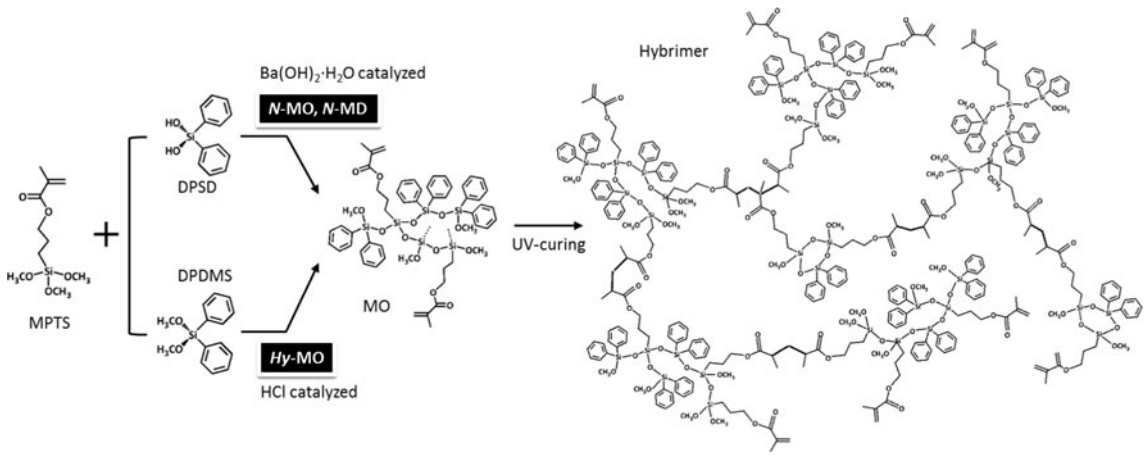

Scheme 1 Synthesis of methacryl-oligosiloxane resin (MO) via a non-hydrolytic (*N*-MO) and a hydrolytic (*Hy*-MO) sol–gel process and fabrication of hybrimer by UV-curing of the MOs. The *N*-MD refers to a non-hydrolytic condensate of MPTS and DPDMS under $Ba(OH)_2{\cdot}H_2O$ (control experiment)

Diphenylsilanediol (DPSD) and diphenyldimethoxysilane (DPDMS) were purchased from Gelest (Morrisville, PA, USA) and TCI (Japan), respectively.

2.2 Synthesis of MO and fabrication of hybrimer

2.2.1 Non-hydrolytic sol–gel synthesis of MO

Non-hydrolytic sol–gel synthesized MO (*N*-MO) was synthesized via a non-hydrolytic sol–gel reaction of MPTS and DPSD. A sample of MPTS (0.1 mol) was mixed with $Ba(OH)_2{\cdot}H_2O$ as the reaction catalyst (0.1 mol% of total silane), and the mixture was reacted with DPSD (0.1 mol) in a two-neck flask at 80 °C under N_2 purging. A viscous transparent resin was obtained after 4 h of reaction. The liquid product was then mixed with the photo-initiator, 2,2-dimethoxy-2-phenylacetophenone (2 wt%) and filtrated through a 0.45 μm Teflon filter. Basic information on the molecular structures can be found in our early works [37].

2.2.2 Hydrolytic sol–gel synthesis of MO

Hydrolytic sol–gel synthesized MO (*Hy*-MO) was synthesized via an acid-catalyzed hydrolytic sol–gel reaction of MPTS and DPDMS. Samples of MPTS (0.1 mol) and DPDMS (0.1 mol) were mixed in a single-neck flask. A 0.5 N HCl aqueous (0.25 mol) solution was then added to the mixture and stirred with a magnetic stirrer for 10 min. The flask was equipped with a reflux condenser. A viscous transparent resin was obtained after 24 h of reaction at 80 °C. The remaining water and methanol were evaporated with a rotary evaporator at 80 °C for 1 h. The liquid product was then mixed with the photo-initiator, 2,2-dimethoxy-2-phenylacetophenone (2 wt%) and filtrated through a 0.45 μm Teflon filter. The final product was prepared as a transparent, higly viscous, colorless resin.

2.2.3 $Ba(OH)_2{\cdot}H_2O$-catalyzed non-hydrolytic sol–gel reaction of MPTS and DPDMS

As a control experiment, we checked the sol–gel reaction in the $Ba(OH)_2{\cdot}H_2O$-catalyzed non-hydrolytic sol–gel reaction of MPTS and DPDMS (*N*-MD) system to gain a fundamental insight into the catalysis of $Ba(OH)_2{\cdot}H_2O$. Samples of MPTS (0.1 mol), DPDMS (0.1 mol), and $Ba(OH)_2{\cdot}H_2O$ (0.1 mol% of total silane) were mixed in a two-neck flask and reacted at 80 °C under N_2 purging for 4 h. The first 4 h failed to produce any sign of a sol–gel reaction, so the reaction was continued for an additional 20 h. A semi-transparent solution of low viscosity was eventually obtained after a total reaction period of 24 h.

2.3 Characterization of MOs

2.3.1 FT-IR analysis

An FT-IR (JASCO, USA) spectroscopic analysis of *N*-MO, *Hy*-MO, and *N*-MD were performed with a resolution of 4 cm^{-1} in a wavelength ranging from 400 to 4,000 cm^{-1}.

2.3.2 Analysis with ^{29}Si NMR

Spectra derived from ^{29}Si NMR of *N*-MO and *Hy*-MO were recorded with a Bruker FT 500 MHz instrument (USA). In the NMR spectra (Fig. 3), the terms D^n and T^n denote the Si levels of DPSD and MPTS, respectively, where the superscript n indicates the number of siloxane bonds of the Si atoms. The chemical shifts of the siloxane bond states are listed in Table 1. The degree of siloxane condensation can be calculated as follows:

$$\text{Degree of siloxane condensation} = \frac{D^1 + 2D^2 + T^1 + 2T^2 + 3T^3}{2(D^0 + D^1 + D^2) + 3(T^0 + T^1 + T^2 + T^3)} \times 100$$

2.3.3 MALDI-TOF mass spectroscopy

A Voyager-DE STR 4700 proteomics analyzer equipped with a nitrogen laser ($\lambda = 337$ nm, pulse width of 3 ns) was used to obtain MALDI-TOF (PerSpetive Biosystem, USA) spectra of *N*-MO and *Hy*-MO.

2.3.4 SANS analysis

SANS analysis was used to characterize the sizes of *N*-MO and *Hy*-MO. In the SANS analysis, the scattering intensity ($I(Q)$) is defined by the following equation, which is derived from the Guinier Law [42]:

$$I(Q) = \rho_0^2 v^2 \exp\left(-\frac{1}{3}Q^2R_g^2\right)$$

where Q is the scattering vector, ρ_0 is the scattering length density of the MO, v is the molar volume of the MO, and R_g is the radius of gyration of the MO.

Table 1 Chemical shifts of silicon according to the bond states

Species	Chemical shifts (ppm)
D^0 (diphenyldimethoxysilane)	−29
D^1	−34
D^2	−36 to −38
T^0	−41 to −42
T^1	−49 to −51
T^2	−57 to −61
T^3	−65 to −69

The R_g values of *N*-MO and *Hy*-MO were calculated with the following equation from the Guinier plots (scattered intensity ($I(Q)$ versus Q^2) in the Guinier region ($0.1 < R_g \times Q < 1$):

$$\ln(I(Q)) = A - \frac{1}{3}Q^2R_g^2$$

2.4 Characterization of hybrimers

For the preparation of hybrimer samples and characterization of the basic properties of hybrimers, *N*-MO and *Hy*-MO resins were UV-cured with a Hg-lamp ($\lambda = 365$ nm, 80 mW/cm^2) under N_2 purging to avoid oxygen quenching. Scheme 1 represent the fabrication of hybrimers with MO resins.

2.4.1 DMA

The viscoelastic responses of the hybrimers were recorded with a DMA (DMA 2980, TA Instruments, Inc., USA). *N*-MO and *Hy*-MO resins were cast into (5 mm × 50 mm × 0.1 mm) sheets. The cast samples were UV-cured for 5 min and heat-treated at 150 °C for 2 h in an ambient atmosphere. The storage modulus (E') and tan δ values were measured within a temperature range of −50 to 200 °C at a ramp rate of 5 °C/min. The vibratory offset force was fixed at 1 N at a frequency of 0.035 Hz.

2.4.2 TGA

The thermal stabilities of the UV-cured *N*-MO and *Hy*-MO were assessed in an N_2 atmosphere with a TGA (Q-50, TA Instruments, Inc., USA). For the sake of accuracy, the N_2 flow rate was fixed at 60 mL/min and the sample masses were fixed at 20 ± 2 mg. The temperature was increased from 25 to 600 °C at a ramp rate of 5 °C/min.

3 Results and discussion

3.1 Characterizations of MO (*N*-MO vs. *Hy*-MO)

As indicated in Scheme 1, we synthesized two different types of MO in the manner described in the "Experimental section". The first type, *N*-MO, was synthesized via the conventional non-hydrolytic sol–gel process with the catalyst $Ba(OH)_2{\cdot}H_2O$. The second type, *Hy*-MO, was synthesized via an acid-catalyzed hydrolytic sol–gel process. We also examined a $Ba(OH)_2{\cdot}H_2O$-catalyzed non-hydrolytic sol–gel reaction between MPTS and DPDMS (*N*-MD) so that we could gain basic insight into the catalysis of $Ba(OH)_2{\cdot}H_2O$. Initially we postulated that the catalysis of $Ba(OH)_2{\cdot}H_2O$ in the non-hydrolytic condensation between DPSD and MTPS (*N*-MO) would be triggered by the deprotonation of the silanols of DPSD at the basic hydroxyl sites on the surface of $Ba(OH)_2{\cdot}H_2O$ crystal. In view of this postulation, it seemed relevant to examine the *N*-MD system under conditions where DPDMS is used instead of DPDS and all other reaction variables are kept the same.

Figure 1 displays FT-IR spectra of *N*-MO, *Hy*-MO, and *N*-MD. There is a notable difference between the *N*-MD system and the *N*-MO system. Peaks corresponding to the siloxane network (Si–O–Si) are clearly apparent in the *N*-MO but not in the *N*-MD [44, 45]. This result indicates that the direct condensation between DPDMS and MPTS, which forms the siloxane network, does not take place in the presence of $Ba(OH)_2{\cdot}H_2O$ even after 24 h of reaction. This result supports our postulated mechanism of $Ba(OH)_2{\cdot}H_2O$; it also supports the view that $Ba(OH)_2{\cdot}H_2O$ acts as a strong basic catalyst which deprotonates molecules at its surface in some typical organic reactions [39, 40]. The results confirm our hypothesis that the limited condensation reaction in *N*-MO is due to the spatial hindrance of the catalytic activity of the solid $Ba(OH)_2{\cdot}H_2O$. In Fig. 1, as anticipated, a substantial amount of the unreacted methoxy groups ($-OCH_3$) can be observed at 2840 cm^{-1} in the case of *N*-MO, whereas there is almost no sign of these methoxy groups in the case of *Hy*-MO [46, 47]. This observation implies that the overall condensation reaction that forms siloxane networks is much more active in *Hy*-MO than in *N*-MO, which is clearly evidenced by a higher degree of siloxane condensation of *Hy*-MO in the subsequent ^{29}Si NMR analysis (see Table 2). On the basis of sol–gel chemistry, the silicon alkoxide groups are rapidly hydrolyzed to silanols prior to condensation under an acid-catalysis. In the *Hy*-MO system, the proton ions

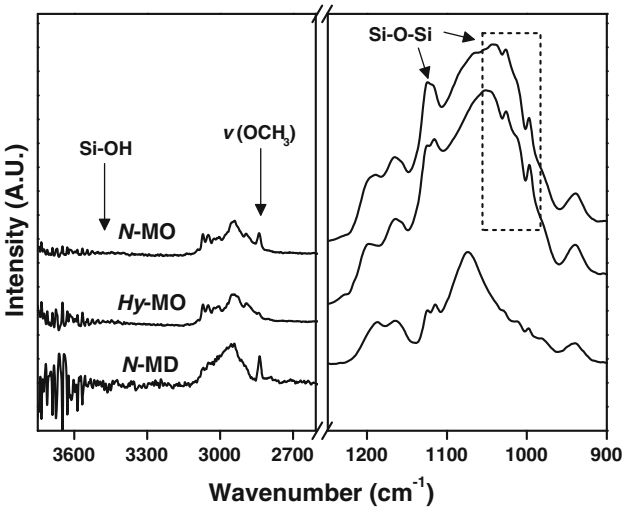

Fig. 1 FT-IR spectra of oligosiloxanes resin synthesized via a non-hydrolytic (*N*-MO), a hydrolytic (*Hy*-MO) sol–gel process and *N*-MD system

dissociated from HCl effectively catalyze this reaction. Unlike the case of *N*-MO, where catalysis can only occur at the solid–liquid interface, the protons are highly mobile and able to catalyze the reaction actively throughout the reaction mixture. Note also in Fig. 1 that Si–OH is absent in both *N*-MO and *Hy*-MO. The related literatures report a strong tendency for most hydroxyl groups (–OH) in DPSD to be converted to methoxy groups (–OCH_3) as a result of esterification reaction with the by-product methanol [37, 38]. This phenomenon is also confirmed by the ^{29}Si NMR spectra (Fig. 2), which show that the unreacted DPSD species (D^0) exist as DPDMS fragments at the chemical shift of 29 ppm (Table 1). The absence of Si–OH in *Hy*-MO can be attributed to a similar trend.

The degree of siloxane condensation in both resins (*N*-MO, *Hy*-MO) and *N*-MD was analyzed with the aid of ^{29}Si NMR. As shown in Fig. 2 and Table 1, there are only two peaks assigned to unreacted monomers of MPTS (T^0) and DPDMS (D^0). This result strongly supports our initial postulation on the catalytic role of $Ba(OH)_2{\cdot}H_2O$. On the other hand, both the D^0 and T^1 species can be clearly observed in *N*-MO but not in *Hy*-MO. Note also that a larger amount of the highly condensed T^3 species can be observed in *Hy*-MO, which implies that *Hy*-MO has a higher degree of siloxane condensation than *N*-MO. As shown in Table 2, the calculated degree of siloxane condensation (see "Experimental section") is 74% for *N*-MO and 88% for *Hy*-MO. This result supports our hypothesis that the siloxane condensation reaction can be hindered in *N*-MO by the limited catalytic activity of the solid catalyst. The steric hindrance may not be significant in the early stage of reaction, which consists mainly of highly mobile monomers, but is likely to become pronounced when the oligomeric species appear as a result of the increased steric effect and low mobility [33]. In fact, the extent of the hindered condensation in the *N*-MO system is expected to be intensified by the sterically bulky MPTS on the basis of the fact that a relatively higher condensation degree is obtained in a non-hydrolytic condensate using vinyltrimethoxysilane or 2-(3,4-epoxycyclohexyl)ethyl trimethoxysilane, which are both sterically smaller than MPTS [43]. The incomplete condensation of *N*-MO induces the non-optimal characteristics of the hybrimer because the macroscale properties (such as thermal stability) of a

Table 2 Basic characteristics of *N*-MO and *Hy*-MO

	R_g (nm)	DOC (%)	$T_{d5\%}$ (°C)	CTE (ppm/°C)
N-MO	0.843	74	309	182
Hy-MO	1.049	88	371	174

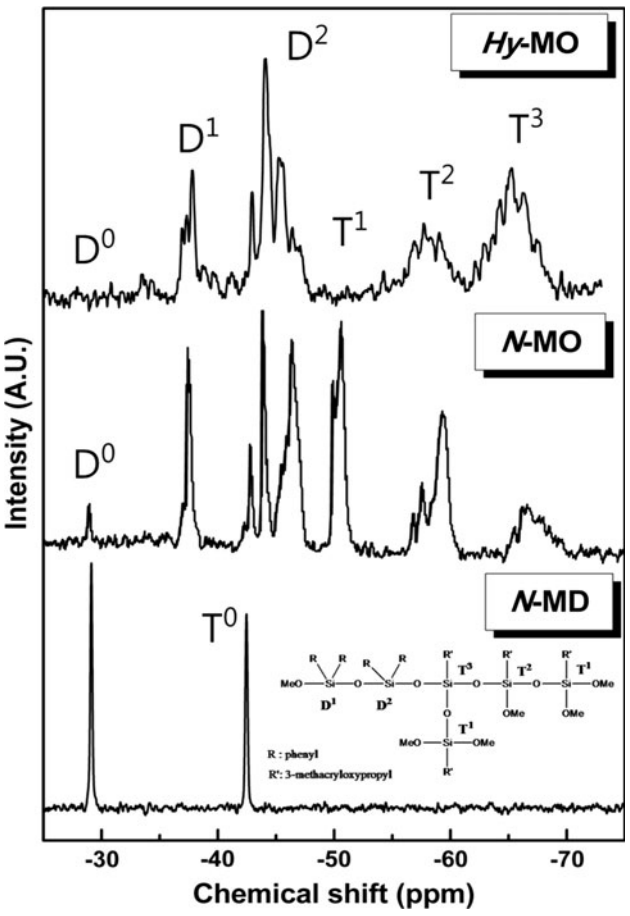

Fig. 2 ^{29}Si NMR spectra of oligosiloxanes resin synthesized via a non-hydrolytic (*N*-MO), a hydrolytic (*Hy*-MO) sol–gel process, and reference product (*N*-MD). The *inset* figure represents the Si atoms with different bond states

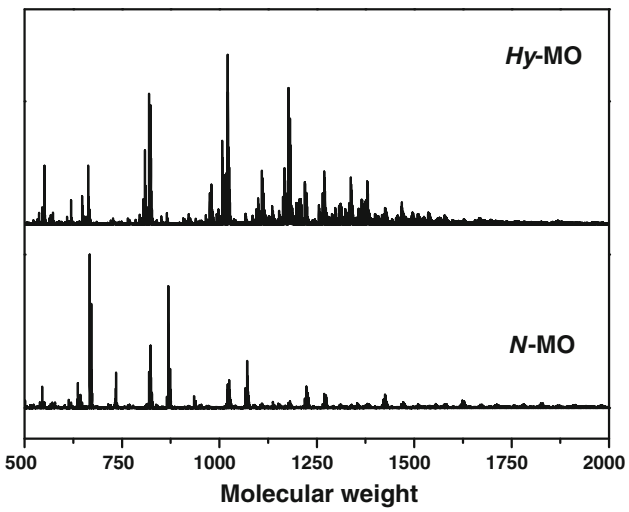

Fig. 3 MALDI-TOF mass spectra of oligosiloxanes resin synthesized via a non-hydrolytic (*N*-MO) and a hydrolytic (*Hy*-MO) sol–gel process

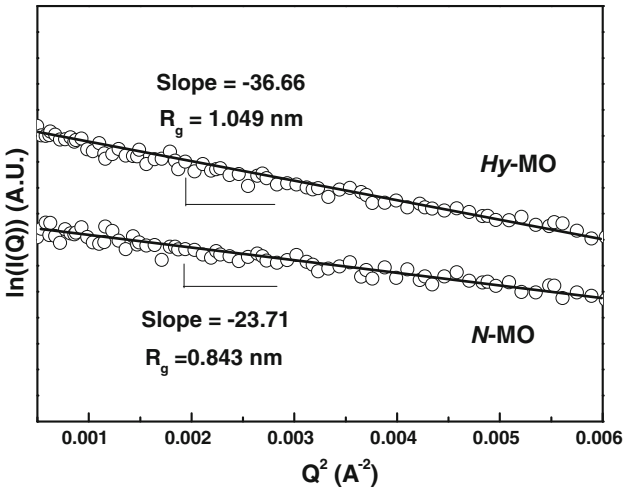

Fig. 4 SANS Guinier plots (ln[I(Q)] vs. Q^2) of oligosiloxanes resin synthesized via a non-hydrolytic (*N*-MO) and a hydrolytic (*Hy*-MO) sol–gel process

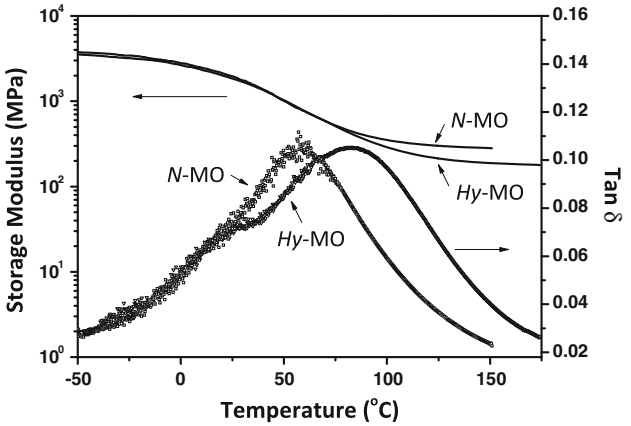

Fig. 5 DMA profile of hybrimers based on oligosiloxanes resin synthesized via a non-hydrolytic (*N*-MO) and a hydrolytic (*Hy*-MO) sol–gel process. Storage modulus (E') and tan δ are plotted

typical OIHM are strongly affected by the inorganic siloxane cores. We observed (as shown in Fig. 6) that the thermal stability of the hybrimer fabricated with *Hy*-MO is significantly enhanced.

The molecular weight and size of both resins were characterized by MALDI-TOF and SANS analyses, respectively. Figure 3 shows that, although there is a distribution of molecular weight in both resins, *Hy*-MO has a larger amount of oligosiloxane condensates with higher molecular weights. Furthermore, as shown in Fig. 4 and Table 2, this result is consistent with the Guinier plots of the SANS analysis, where *Hy*-MO has a larger R_g value (1.049 nm) than *N*-MO (0.843 nm).

3.2 Characterizations of hybrimer (*N*-MO vs. *Hy*-MO)

For characterization of the basic properties of hybrimer, we prepared two types of hybrimer samples on the basis of UV-induced polymerization of *N*-MO and *Hy*-MO (Scheme 1). First, the viscoelastic properties were characterized by DMA to investigate their cross-linked network structures. Figure 5 displays the DMA curves of both hybrimers; the storage modulus (E') and tan δ are plotted with temperature. Note that both cases have similar E' profiles over the entire temperature scan range except that the E' value of *Hy*-MO is slightly lower in its rubbery state. This result indicates that they both have similar cross-linked network structures; the viscoelastic (or thermo-mechanical) response of polymeric materials is directly related to the overall network structure and network cross-linking density [18, 21, 23]. In both the *N*-MO and *Hy*-MO cases, the glassy and rubbery plateaus can be clearly observed. Moreover, the E' value decreases gradually over a wide temperature range and the extent of the decrease is less than an order of magnitude; this type of behavior is not generally observed in typical organic polymers. Organic polymers usually show an abrupt decrease in E' and sharp tan δ peaks at their glass transition temperature (T_g). This result implies that hybrimers have highly cross-linked network structures; that is, the oligosiloxane cores are completely isolated from each other by short methacryl chain segments [23]. Thus, we can deduce that the macroscopic viscoelastic behavior of hybrimers is the sum of the thermal relaxation motions of the inorganic siloxane cores and the cross-linked methacryl chain segments.

Although the *N*-MO and *Hy*-MO cases both have similar E' profiles, they have different tan δ curves. *N*-MO has a single tan δ peak with a maximum value at T_g (50 °C); in contrast, the main T_g of *Hy*-MO shifts to a higher temperature point (80 °C) with a small shoulder at 25 °C. In light of the above background, this result can be attributed to the fact that *Hy*-MO has highly condensed oligosiloxanes, which are more resistant to thermal relaxation. This behavior is also confirmed by the lower coefficient of thermal expansion of *Hy*-MO in the dilatometric analysis (see Table 2 and Fig. S1 in Supplementary Information), because the molecular backbone's resistance in thermal motion is directly related to the thermal expansion of the material.

The major advantage of using highly condensed *Hy*-MO as a building block of hybrimer is the fact that it has a higher level of thermal stability than conventional *N*-MO. Figure 6 displays the TGA profiles from which the 5% weight loss temperature ($T_{d5\%}$) can be compared (Table 2). Note that the thermal stability of *Hy*-MO ($T_{d5\%}$ = 371 °C) is significantly more enhanced than *N*-MO ($T_{d5\%}$ = 309 °C). The enhanced thermal stability of *Hy*-MO can be attributed to the highly condensed *Hy*-MO and the fact that there is no unreacted monomer traces (D^0 species in Fig. 2) that can be thermally decomposed, even at a low temperature.

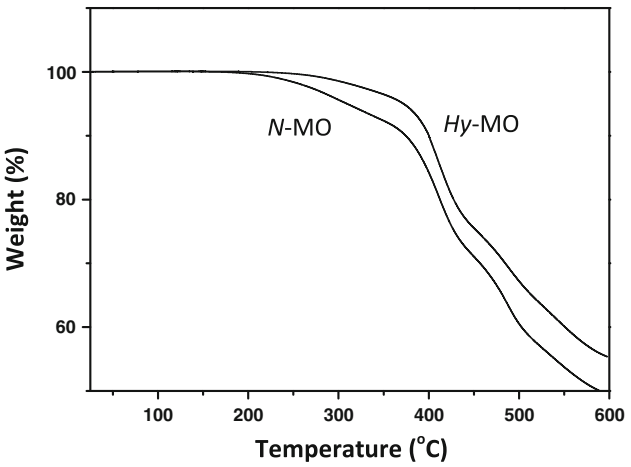

Fig. 6 TGA profile of hybrimer based on oligosiloxanes resin synthesized via a non-hydrolytic (*N*-MO) and a hydrolytic (*Hy*-MO) sol–gel process (measured under N_2 atmosphere)

4 Conclusion

In this study, we report on an acid-catalyzed hydrolytic sol–gel synthesis of MO (*Hy*-MO) for the purpose of preparing a thermally stable hybrimer. Compared to conventional non-hydrolytic sol–gel condensates (*N*-MO) made with a $Ba(OH)_2 \cdot H_2O$ solid catalyst, which induces spatial hindrance in the catalysis, *Hy*-MO has a higher degree of siloxane condensation and a large molecular size and weight due to the active catalytic activity of labile proton ions. As a result, the Hy-MO hybrimer as significantly enhanced thermal stability.

Acknowledgments This work was supported by the National Research Foundation of Korea (NRF) grant funded by the Korea government (MEST) (No. 2011-0006406). The authors gratefully thank the Korea Basic Science Institute for NMR and MALDI-TOF MS spectra measurements.

References

1. Jones RG, Ando W, Chojnowski J (2000) Silicon-containing polymers. Kluwer Academic Publishers, Dordrecht, Netherlands
2. Mark JE, Lee C, Bianconi PA (1995) Hybrid organic-inorganic composites, ACS Symposium Series 585
3. Kickelbick G (2007) Hybrid materials. WILEY-VCH, Germany
4. Comez-Romero P, Sanchez C (2004) Functional hybrid materials. WILEY-VCH, Germany
5. Abe Y, Gunji T (2004) Prog Polym Sci 29:149–182
6. Sanchez C, Lebeau B, Ribot F, In M (2000) J Sol–Gel Sci Technol 19:31–38
7. Buestrich R, Kahlenberg F, Popall M (2001) J Sol–Gel Sci Technol 20:181–186
8. Houbertz R, Frohlich L, Popall M, Streppel U, Dannberg P, Brauer A, Serbin J, Chichkov BN (2003) Adv Eng Mater 5:551
9. Kim WS, Kim KS, Eo YJ, Yoon KB, Bae BS (2005) J Mater Chem 15:465–469
10. Kang DJ, Kim WS, Bae BS (2005) Appl Phys Lett 87:22106
11. Kang DJ, Jeong JP, Bae BS (2006) Opt Express 14:8347–8353
12. Kang DJ, Bae BS (2007) Acc Chem Res 40:903–912
13. Kros A, Gerritsen M, Sprakel V, Sommerdijk N, Jansen J, Nolte R (2001) Sens Actuators B 81:68–75
14. Schottner G (2001) Chem Mater 13:3422–3435
15. Nagase T, Hamada T, Tomatsu K, Yamazaki S, Kohayashi T, Murakami S, Matsukawa K, Naito H (2010) Adv Mater 22:4706–4710
16. Mammeri F, Le Bourhis E, Rozes L, Sanchez C (2005) J Mater Chem 15:3787–3811
17. Oh J-H, Kwak S-Y, Yang S, Bae BS (2010) ACS Appl Mat Interfaces 2:913–918
18. Ro HW, Soles CL (2011) Mater Today 14:20–33
19. Shim JH, Lee S-I, Lee H-J, Kasica R, Kim H-M, Soles CL, Kim K-B, Yoon DY (2010) Chem Mater 22:3021–3023
20. Ro HW, Popova V, Chen L, Forster AM, Ding Y, Alvine KJ, Krug DJ, Laine RM, Soles CL (2011) Adv Mater 23:414–420
21. Choi J, Harcup J, Yee AF, Zhu Q, Laine RM (2001) J Am Chem Soc 123:11420–11430
22. Choi J, Yee AF, Laine RM (2003) Macromolecules 36:5666–5682
23. Jin J, Yang S, Bas BS (2011) Polym Chem 2:168–174
24. Livage J (1997) Curr Opin Solid State Mater Sci 2:132–138
25. Wen J, Wilkes GL (1996) Chem Mater 8:1667–1681
26. Brinker CJ, Scherer GW (1990) Sol–gel science. Academic Press, New York
27. Wilkes GL, Orler B, Huang H (1985) Polym Prepr 26:300
28. Schmidt H (1985) J Non-Cryst Solids 73:681
29. Bae BS (2004) J Sol–Gel Sci Technol 31:309–315
30. Lee KJ, Jin J, Bae BS, Magnusson R (2009) Opt Lett 34:2510–2512
31. Kim J-S, Yang S, Bae BS (2010) Chem Mater 22:3549–3555
32. Yang S, Kim J-S, Jin J, Kwak S-Y, Bae BS (2010) J Appl Polym Sci 117:2140–2145
33. Yang S, Kwak S-Y, Jin J, Bae BS (2009) ACS Appl Mat Interfaces 1:1585–1590
34. Jung KH, Bae J-Y, Yun H-G, Kang MG, Bae BS (2011) ACS Appl Mat Interfaces 3:293–298
35. Jung KH, Bae J-Y, Park SJ, Yoo S, Bae BS (2011) J Mater Chem 21:1977–1983
36. Jin J, Ko J-H, Yang S, Bae BS (2010) Adv Mater 22:4510–4515
37. Eo YJ, Lee TH, Kim SY, Kang JK, Han YS, Bae BS (2005) J Polym Sci B 43:827–836
38. Kim SY, Augustine S, Eo YJ, Bae BS, Woo SI, Kang JK (2005) J Phys Chem B 109:9397–9403
39. Aguilera A, Alcantara AR, Marinas JM, Sinisterra JV (1987) Can J Chem 65:1165–1171
40. Climent MS, Marinas JM, Mouloungui Z, Le Bigot Y, Delmas M, Gaset A, Sinisterra JV (1989) J Org Chem 54:3695–3701
41. Lee D-W, Park Y-M, Lee K-Y (2009) Catal Surv Asia 13:63–67
42. Roe RJ (2000) Methods of X-ray and neutron scattering in polymer science. Oxford University Press, Oxford
43. Jung KH, Bae BS (2008) J Appl Polym Sci 108:3169–3176
44. Innocenzi P, Brusatin G, Guglielmi M, Bertani R (1999) Chem Mater 11:1672–1679
45. Ou DL, Seddon AB (1997) J Non-Cryst Solids 210:187–203
46. Sivoththaman S, Jeyakumar R, Ren L, Nathan A (2002) J Vac Sci Technol 20:1149–1153
47. Shirosakia Y, Tsurua K, Hayakawa S, Osaka A, Lopes MA, Santos JD, Fernandes MH (2005) Biomaterials 26:485–493